Nanoscale

Accepted Manuscript

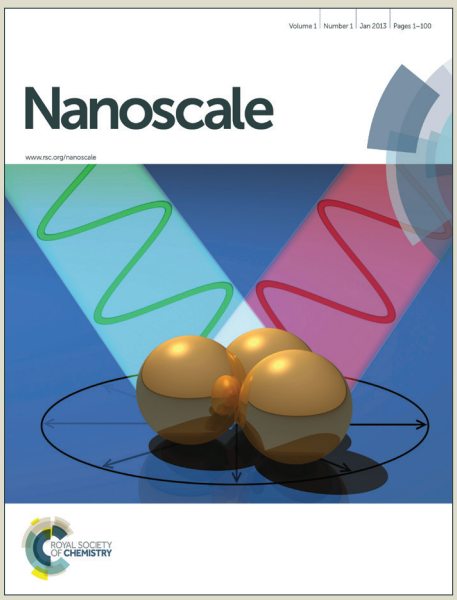

ROYAL SOCIETY OF CHEMISTRY

www.rsc.org/nanoscale

Journal Name

RSCPublishing

ARTICLE

A simple method to adjust the morphology of gradient three-dimensional PTB7-Th:$PC_{71}BM$ polymer solar cells

Ling Zhao[a,b], Suling Zhao[a,b,c], Zheng Xu[a,b], Qianqian Yang[a,b], Di Huang[a,b] and Xurong Xu[a,b]

Cite this: DOI: 10.1039/xoxxoooooox

Received ooth January 2012,
Accepted ooth January 2012

DOI: 10.1039/xoxxoooooox

www.rsc.org/

The multiple interfaces are necessary for exciton separation in bulk heterojunction (BHJ) solar cells and the continuous pathways for carrier transportation in the donor:acceptor blend films, especially along vertical direction, for efficient charge collection. Therefore film morphology is critically important to satisfy both in constructing high performance organic solar cells (OSCs). In this work, cooperative effect of solvent additives and solvent flux treatment to the film morphology was confirmed. Furthermore, the correlation between single processing parameter and resulting morphology has been investigated. Our results show that the film morphology can be tuned by changing the volume fraction of solvent additive. Beyond that, after solvent flux treatment, the OSC performance was improved significantly, as short circuit current density (J_{SC}) increases from 13.85 mA/cm^2 to 15.17 mA/cm^2 and fill factor (FF) from 62.9% to 65.7%, simultaneously. As a result, power conversion efficiency (PCE) increases from 6.79% to 7.67%. The favourable morphology was further investigated using the time-of-flight secondary-ion mass spectroscopy (TOF-SIMS), the atomic force microscopy (AFM).

1. Introduction

Polymer bulk heterojunction (BHJ) solar cells, as an alternative technology of green energy source, have attracted much attention due to their advantages, such as low processing cost, large area, environmentally friendly, flexible and light weight, over their inorganic counterparts.[1-5] The morphology of BHJ films plays a very important role in the whole performance in BHJ organic solar cells (OSCs), to achieve high power conversion efficiency (PCE), the BHJ films must have multiple interfaces for efficient charge separation and long percolation pathways for efficient charge transport.[6,7] Usually for polymer:fullerene blend films, the donor and acceptor molecules are intimately mixed, as shown in Fig. 1(a), enabling efficient charge transfer from donor to acceptor molecules. To facilitate charge transport, however, it requires moderate phase separation to form the percolation paths for charge extraction. Because the effective charge collection occurs along the vertical direction, the gradient distribution of donor and acceptor in the bulk film plays an important role.[8] The following parameters have been identified experimentally as most significant for their influence on the nanoscale morphology in these BHJ films: 1) the molecular interaction of donor and acceptor materials; 2) the weight ratio of donor material to acceptor material; 3) the solvent used for solution processing; 4) necessary treatments, such as thermal/solvent annealing.[9-17] These methods address both donor/acceptor interfaces and continuous pathways for carrier transportation in vertical direction, and mitigates the charge recombination,[18] Yet to achieve ideal morphology for polymer BHJs, further approaches are desperately needed.

Three-dimensional structure of bulk heterojunction is shown in Fig. 1 (b). The BHJ active layer should consist of a donor (p-type) rich layer near the high work function anode and an acceptor (n-type) rich layer near the low work function cathode, and a mixed layer in between, to maximize the charge extraction efficiency. In the polymer:fullerene blend systems, Jo et al demonstrated that solvent annealing could force the fullerene derivative PCBM molecules to migrate or diffuse toward the top surface of the BHJ composite films, which induces a new vertical component distribution in the active layer.[19] Thermal annealing step could increases the PCBM concentration on the top surface of the active layer due to PCBM diffusion, and hence this improved vertical morphology contributes to the increase in efficiency.[20] Moule´ et al have built three-dimensional networks upon the P3HT nanofiber by using the self-assembly of P3HT into aligned structures.[21,22] More recently, Xiao et al. have reported a method to effectively form the graded BHJ by a very simple solvent-fluxing process which is applicable to BHJ films in which solvent additives are also involved.[18]

The cooperation of solvent additives and solvent flux treatment has been proved to be a successful method to form graded BHJ structure. However, the adjustments of the morphology of gradient BHJ was rarely reported. Previous study shows that 1,8-diiodooctane (DIO) is a better solvent for fullerene-derivatives (>120 mg/mL for PCBM) than traditional solvents, such as chlorobenzene (CB), because of their strong interactions caused by the partial negative charge of iodine in DIO and electro-deficiency of fullerene-derivatives. Methanol was chosen as fluxing solvent for the following reasons: 1) low boiling point; 2) does not dissolve either fullerene-derivatives or semiconducting polymers; 3) mixes very

well with DIO. Xiao et al. also reported that DIO remains in the blend film due to its high boiling temperature of 333 ℃.[18] So methanol fluxing helps not only to optimize the multiple interfaces and continuous pathways for carrier transportation, but to remove the high-boiling point solvent. In this paper, cooperative effect of DIO and methanol flux treatment to the film morphology was confirmed. Furthermore, the correlation between volume fraction of DIO and resulting morphology has been investigated. And it reveal that the morphology of gradient three-dimensional PTB7-Th:$PC_{71}BM$ polymer solar cells could be adjusted by changing the volume fraction of DIO. Different films and devices were prepared to study the effect of the morphology of PTB7-Th:$PC_{71}BM$:

Film 1: PTB7-Th:$PC_{71}BM$:DIO(0%),vacuum dried
Film 2: PTB7-Th:$PC_{71}BM$:DIO (0.5%),vacuum dried
Film 3: PTB7-Th:$PC_{71}BM$:DIO (1%),vacuum dried
Film 4: PTB7-Th:$PC_{71}BM$:DIO (3%),vacuum dried
Film 5: PTB7-Th:$PC_{71}BM$:DIO (5%),vacuum dried
Film 6: PTB7-Th:$PC_{71}BM$:DIO (0%), methanol fluxed then vacuum dried
Film 7: PTB7-Th:$PC_{71}BM$:DIO (0.5%), methanol fluxed then vacuum dried
Film 8: PTB7-Th:$PC_{71}BM$:DIO (1%), methanol fluxed then vacuum dried
Film 9: PTB7-Th:$PC_{71}BM$:DIO (3%), methanol fluxed then vacuum dried
Film 10: PTB7-Th:$PC_{71}BM$:DIO (5%), methanol fluxed then vacuum dried

Device 1:ITO/PEDOT:PSS /film1/PFN/Al
Device 2:ITO/PEDOT:PSS /film2/PFN/Al
Device 3:ITO/PEDOT:PSS /film3/PFN/Al
Device 4:ITO/PEDOT:PSS /film4/PFN/Al
Device 5:ITO/PEDOT:PSS/film5/PFN/Al
Device 6:ITO/PEDOT:PSS /film6/PFN/Al
Device 7:ITO/PEDOT:PSS /film7/PFN/Al
Device 8:ITO/PEDOT:PSS /film8/PFN/Al
Device 9:ITO/PEDOT:PSS/film9/PFN/Al
Device 10:ITO/PEDOT:PSS/film10/PFN/Al

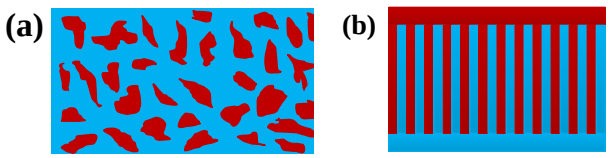

Fig. 1 (a) Illustration of the morphology of regular BHJ devices, (b) Illustration of the morphology of three-dimensional BHJ devices.

2. Experimental details

2.1 Materials

PTB7-Th from 1-material, Poly(9,9-bis(3'-(N,N-dimethyl)-propyl-2,7-fluorene)- alt-2,7-(9,9-dioctylfluorene)) (PFN-P1) from 1-material, [6,6]-phenyl C71butyric acid methyl ester ($PC_{71}BM$) from Nano-C (99.9% purity), 1,8-diodooctane from Sigma-Aldrich (98.0% purity), chlorobenzene (CB) from J&K Scientific (99.0% purity), methanol from J&K Scientific (99.0% purity).

2.2 Device Fabrication

The cells were prepared on glass/ITO substrates. Firstly, the ITO-coated glass substrates were cleaned in ultrasonic bath with washing liquor, acetone, ethanol and deionized water successively for 20 min. Then the cleaned ITO substrates were dried by N_2 and followed by a UV processing for 6 min. A highly conducting polymer PEDOT:PSS was spin coated onto the treated ITO substrates from an aqueous solution, then these ITO coated with PEDOT:PSS were annealed in air at 150 ℃ for 10 min. Thirdly, the CB solution composed of PTB7-Th and PC71BM was spin-coated to form the active layer on the top of the PEDOT:PSS layer. Fourthly, the active layers were fluxed by methanol. Fifth, the PFN was spin-coated on the active layer. Subsequently, the aluminum cathode was deposited via thermally evaporation method in a vacuum chamber respectively. The photoactive area of the cells is 0.06 cm^2, which is defined by the vertical overlap of ITO anode and Al cathode. All the measurements were performed at room temperature in air without any device encapsulation. Fig. 2 shows the structure and the energy level diagram of devices.

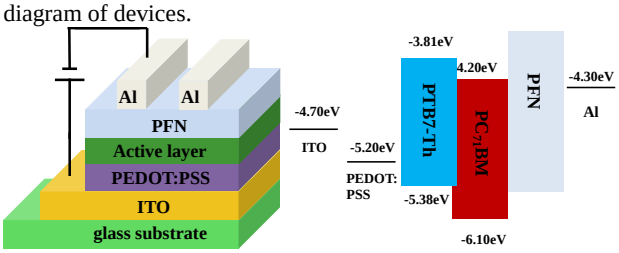

Fig. 2 Structure and energy level diagram of the OSCs.

2.3 Measurements

The absorption spectra of films were measured with a Shimadzu UV-3101 PC spectrometer. The morphology of films was investigated by atomic force microscopy (AFM) using a multimode Nanoscope IIIa operated in tapping mode.

Secondary ion mass spectrum was obtained using a time-of-flight secondary ion mass spectrometer TOF-SIMS 5 from ION-TOF GmbH (Munster, Germany). A Bi_1^+ liquid metal ion gun operating at a 30keV beam voltage with a 45 ° incident angle was used. The depth profiling experiment was performed using a gas cluster ion gun $Ar_{1700}^+$with an analyzed area of 100 ×100 μm inside an etching area of 500 × 500 μm. All analyses were carried out at 256 × 256 pixels. Charge compensation with an electron flood gun was used during the analysis cycles. Negative ion mode spectra were calibrated on the C^-, CH^-, C_2^- and C_2H^- peaks.

The current density–voltage (J–V) of devices was measured using a Keithley 4200 semiconductor characterization system and ABET Sun 2000 solar simulator. The external quantum efficiency (EQE) spectra were measured on Zolix Solar Cell Scan 100.

3. Results and discussion

3.1 Formation of the gradient three-dimensional structure

In order to confirm the formation of the gradient three-dimensional structure, PTB7-Th:$PC_{71}BM$ films dried under vacuum and fluxed with methanol have been investigated by time-of-flight secondary ion mass spectrometer (TOF-SIMS) to measure the yield of fluorine and sulfur ions (F^- and S^-) which are unique to PTB7-Th. So we could study the change of distribution of PTB7-Th and $PC_{71}BM$ in vertical direction by analyzing the yield variation of F^- and S^- distribution in whole BHJ along with the sputter time. The TOF-SIMS results in the vertical direction of film 3 and 8 are shown in Fig. 3. In Fig. 3, the yield of F^- and S^- of the film after methanol fluxing are less than that of the film dried in vacuum in the beginning time which corresponds to the surface of the BHJ layer. After 55 seconds and 75 seconds, respectively, the yield of F^- and S^-

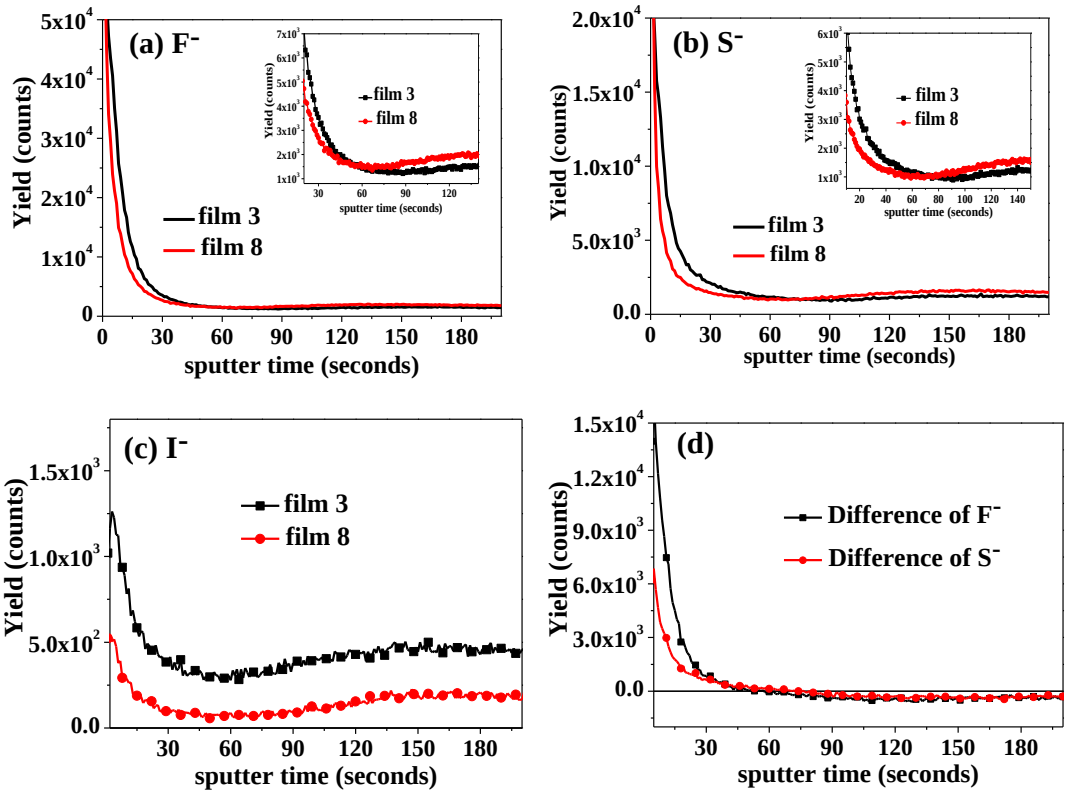

Fig. 3 Depth profile of films 3 and 8 measured by TOF-SIMS: (a) F^-, (b) S^-, (c) I^-, and (d) the difference of F^- and S^-.The inset Fig. is an amplification of local curves.

of the film after methanol fluxing are more than that of the film dried in vacuum respectively. It is clear shown in insert two Figures that there is a junction for the yield of F^- and S^- for two films respectively. Furthermore, we also find that the yield of I^- of the film after methanol fluxing (film 8) are less than that of the film dried in vacuum (film 3), as shown in Fig. 3(c). This phenomenon indicate that methanol fluxing help to remove the DIO. In Fig. 3 (d), the difference of F^- and S^- are defined as the yield difference of F^- and S^- between film 3 and film 8, respectively. Obviously, at the beginning of sputter time, the difference of F^- and S^- are positive and decrease along with the sputter time. While the difference of F^- and S^- become negative respectively after 55 seconds and 75 seconds, and then keep as constants. It means that the content of PTB7-Th closing to the surface of the film after methanol fluxing is less than that of the film dried at vacuum, while the content of PTB7-Th within the film after methanol fluxing is more than that of the film dried at vacuum. The donor and acceptor distribution in BHJ film dried at vacuum always is considered as uniformly. Therefore, the results of Fig. 3(d) give an evidence that the distribution of donor and acceptor molecule in the film after methanol fluxing are gradient distributed in the vertical direction. Therefore, we make a reasonable conclusion that $PC_{71}BM$ migrates or diffuses toward the top surface of the BHJ films after methanol fluxing. Meanwhile, it demonstrates the formation of gradient BHJ OSCs.

The lateral PTB7-Th distributions images in the top and within BHJ films with and without methanol fluxing generated by TOF-SIMS measurements are shown in Fig. 4 and Fig. 5. In Fig. 4, the yield of F^- on the top of the film (at 5 second) decreased from 6.543×10^4 (Fig. 4(a)) to 5.029×10^4 (Fig. 4(b)) after methanol-fluxing, while the yield of F^- within the film (at 150 second) increased from 3.084×10^3 (Fig. 4(c)) to 3.916×10^3 (Fig. 4(d)). After methanol-fluxing, the yield of S^- on the top of the film (at 5 second) reduces from 2.715×10^4 (Fig. 5(a)) to1.719×10^4 (Fig. 5(b)), while the yield of S^- within the film (at 150 second) increases from 2.417×10^3 (Fig. 5(c)) to 3.102×10^3 (Fig. 5(d)). So we can verify that the PTB7-Th content in the top surface of the film decreases after methanol fluxing, meanwhile increases within the film. In other words, the $PC_{71}BM$ content increases in the surface of the film after methanol fluxing. These results are in excellent agreement with that shown in Fig. 3. From Fig. 4, we could also see that the distribution of F^- for films 3 and 8 are different at the same sputter time. And the analogous phenomenon could be seen in Fig. 5 for S^-. All these results show that methanol fluxing could cause changes in the distribution of PTB7-Th and $PC_{71}BM$ in two-dimensional plane. Based on the results gotten from Fig. 3, Fig. 4 and Fig. 5, we reach the opinion that we have succeeded in preparing gradient three-dimensional BHJ OSCs. And the formation processes of gredient three-dimensional BHJ are summerized as folows: Firstly, PTB7-Th:$PC_{71}BM$:DIO solution was spin coating on the top of ITO/PEDOT:PSS substrate, and DIO grasped fullerene derivatives into nano-droplets during the solvent evaporation. When the wet blended film was fluxed by methanol, methanol does not dissolve fullerene-derivatives or semiconducting polymers but mix DIO very well. Therefore, after dripping methanol on the top of the blended film, methanol quickly penetrated into the wet film by dissolving DIO, in which $PC_{71}BM$ nano-droplets were formed. Then, along with the evaporation of methanol, DIO was extracted from inside of the active layer toward the surface. During this process, some fullerene-derivatives dissolved in DIO were brought to the film

surface and thus forms the gradient distribution of PC71BM in the vertical direction. Finally, while methanol was spun off of the surface of the film, DIO was fluxed away by methanol, and the deeper colored graded BHJ films after methanol dried were obtained.

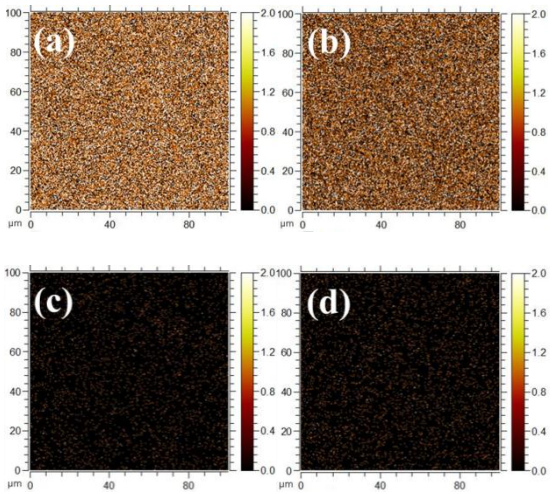

Fig. 4 TOF-SIMS images of F^- a) film 3 at 5-second scan, b) film 8 at 5-second scan, c) film 3 at 150-second scan, d) film 8 at 150-second scan. In images (a), (b), (c) and (d) the spots denote F^- corresponding to the PTB7-Th molecules.

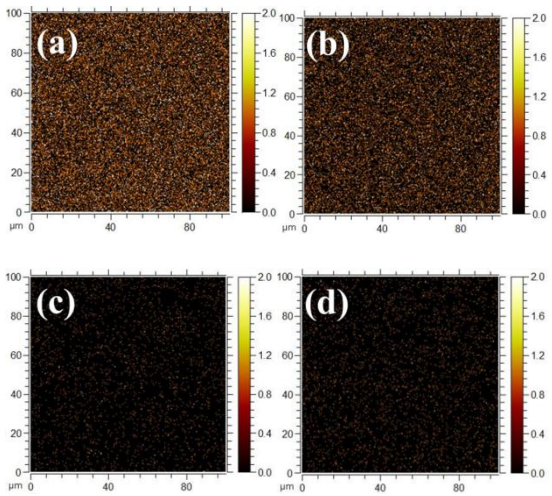

Fig. 5 TOF-SIMS images of S^- a) film 3 at 5-second scan, b) film 8 at 5-second scan, c) film 3 at 150-second scan, d) film 8 at 150-second scan. In images (a), (b), (c) and (d) the spots denote S^- corresponding to the PTB7-Th molecules.

3.2 Gradient three-dimensional PTB7-Th:$PC_{71}BM$ with adjustable morphology

It is confirmed in above discussion that gradient three-dimensional BHJ was prepared by using cooperative effect of solvent addtives and solvent flux treatment. In addition, the volume fraction of DIO doped in BHJ films plays an important rule to effect the morphology of gradient three-dimensional BHJ films, which is investigated by the atomic force microscopy (AFM). Fig. 6 shows surface topographic AFM images of PTB7-Th:$PC_{71}BM$ films at PEDOT:PSS layers: (a) film 6, (b) film 7, (c) film 8,(d) film 9 and (e) film 10. The root mean square roughness (R_{ms}) of the PTB7-Th:$PC_{71}BM$ made from different DIO volume fraction are 17.921 nm (film 6), 8.184 nm (film 7), 9.780 nm (film 8),20.182 nm (film 9) and 29.008 nm (film 10), respectively. In Fig. 6, film 7 has the smoothest surface, and film 10 comes last. These results are consistent with the result of Rms. After methanol fluxing, all films with DIO show roughness surface and their domain size increases with the increase of DIO volume fraction. It is because that DIO helps the phase separation of BHJ. This phenomenon indicates that control the morphology of gradient three-dimensional BHJ film by changing the volume fraction of DIO is feasible.

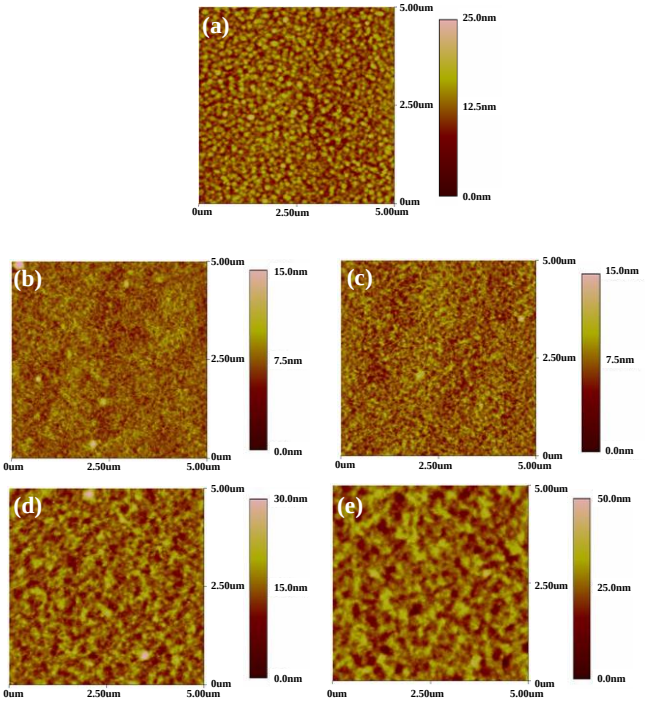

Fig. 6 Surface topographic AFM images of PTB7-Th:$PC_{71}BM$ films atop a PEDOT:PSS layer:(a) film 6, (b) film 7, (c) film 8,(d) film 9 and (e) film 10.

Then we prepared all devices according above optimized parameters to compare their performance (see the supporting information). Fig. 7 shows the J-V characteristics of devices and the detailed performance parameters under different DIO volume fraction are summarized in Table 1. As shown in Fig. 7(a), after the doping of DIO with volume fraction of 3%, the whole performance of OSCs significantly improved, J_{SC} increases from 11.55 mA/cm^2 to 14.10 mA/cm^2 and FF increases from 48.29% to 63.74%, simultaneously, PCE increases from 4.46% to 7.01%. From Fig. 7 we could see that not all the cells with methanol fluxing show a better performance than device vacuum dried, and device 8 shows the best performance. This indicates that the morphology of gradient three dimensional PTB7-Th:$PC_{71}BM$ plays a very important role in the whole performance. By contrasting devices 3 and 8, after the methanol treatment, the whole performance of OSCs significantly improved, J_{SC} increases from 13.85 mA/cm^2 (device 3) to 15.17 mA/cm^2 (device 8) and FF increases from 62.86% (device 3) to 65.68% (device 8), simultaneously, PCE increases from 6.79% (device 3) to 7.67% (device 8). The increase in J_{SC} and FF implies lower series resistance (R_S) (decreases from 17.25 Ω•cm^2 to 6.61 Ω•cm^2 after methanol fluxing).[23] This R_S reduction can be attributed

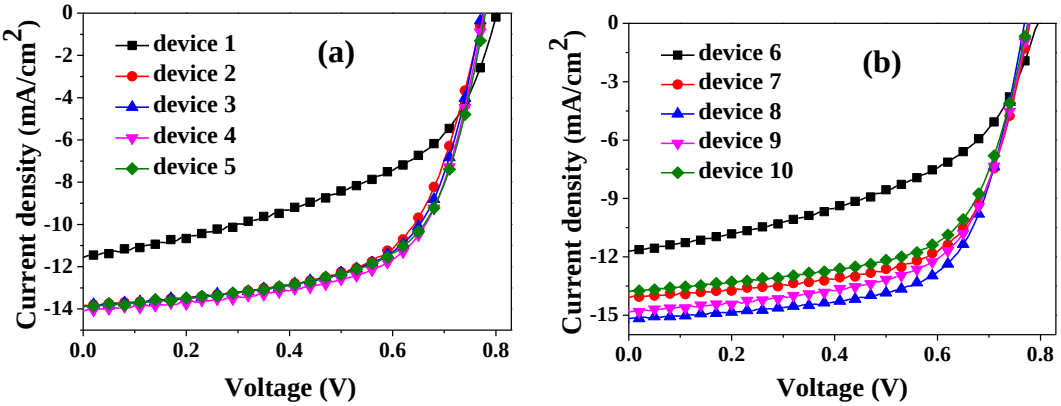

Fig. 7 (a) J-V characteristics of devices vacuum dried with different DIO volume fraction, (b) J-V characteristics of devices methanol fluxing with different DIO volume fraction.

Table 1 Performance parameters of vacuum dried (reference device) and methanol fluxing OSCs with different DIO volume fraction.

Device	J_{SC} (mA/cm^2)	J_{SC}(calc.) (mA/cm^2)	V_{OC}(V)	FF (%)	PCE (%)	Ave PCE (%)
1	11.55	11.43	0.80	48.29	4.46	4.44
2	13.82	13.46	0.78	62.07	6.69	6.68
3	13.85	13.55	0.78	62.86	6.79	6.76
4	14.10	14.01	0.78	63.74	7.01	6.97
5	13.88	13.58	0.78	63.33	6.86	6.89
6	12.19	11.88	0.80	47.68	4.45	4.42
7	14.09	13.79	0.78	64.23	7.06	7.04
8	15.17	14.40	0.77	65.68	7.67	7.66
9	14.83	14.25	0.78	62.76	7.26	7.25
10	13.77	13.33	0.77	63.67	6.75	6.74

The averaged PCE values are calculated based on 30 cells.

to an improved interface morphology, since for the gradient three-dimensional devices, the PFN side (cathode) is $PC_{71}BM$-rich, while the opposite PEDOT:PSS side (anode) is PTB7-Th-rich, and thus charge carrier recombination can be substantially reduced. The Rsh increases from an initial value of 572.84 Ω•cm^2 to 936.94 Ω•cm^2 after methanol fluxing. The larger R_{sh} also indicates a lower charge carrier recombination in active layer.[24] But for device 10, the performance of device decreased little compared with device 5, which may be caused by interface issues between BHJ layer and cathode. Film with lager R_{ms} inevitably causes the charge recombination at the interface between the BHJ and the electrode.

For further undertand the effect of gradient three-dimensional morphology, the champion cells (device 8) and corresponding refrence cell (device 3) are researched systematically. For the entire wavelength range, device 8 exhibits a higher external quantum efficiency (EQE) than device 3, as shown in Fig. 8 (a). In addition, there is no noticeable difference in the shape of EQE spectra among these devices, while they display different efficiencies of photons into electrons. The EQE of OSC with methanol fluxing exhibits the highest efficiency around 460nm in all devices, which is approximately 70%. The absorption intensity of the films vacuum dried and methanol fluxing were shown in Fig. 8 (b). No distinct variation of the absorption peaks of the films 3 and 8 could be observed, especial in the longer wavelength range. The absorption spectrum of film 8 increase a little compared with film 3 when wavelength < 380 nm. We infer that the increase of absorption spectrum of PTB7-Th:$PC_{71}BM$ blend films between 300nm and 380nm is probably caused by the diffusion of $PC_{71}BM$ toward the top surface of the BHJ films. According to the relationship between EQE and internal quantum efficiency (IQE) (Equation (1)):

$$IQE(\lambda) = EQE(\lambda)/Abs_{AL}(\lambda) \quad (1)$$

Where Abs_{AL} is the absorption of the active layer.[25,26] Combined with the results of Fig. 8, it is concluded that the IQE of device 8 is significantly increased compared with that of device 3, and this indicates continuous pathways for carrier transportation and larger-area PTB7-Th:$PC_{71}BM$ interfaces after the methanol fluxing. Therefore, the improved performance of OSCs after methanol fluxing is mainly resulted from the improved charge transportation and collection because of the gradient phase mixing of active layer.

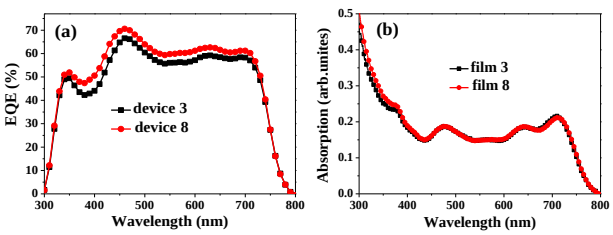

Fig. 8 (a)EQE of OSCs based on PTB7-Th:$PC_{71}BM$ vacuum dried and methanol fluxing, (b) absorption spectrum of PTB7-Th:$PC_{71}BM$ films vacuum dried and methanol fluxing.

Carrier mobility is a physical quantity used to represent the speed of carrier transport. The charge carrier transport in PTB7-Th:$PC_{71}BM$ is studied by using the space charge limited current (SCLC) approach.[27,28] According to the Mott-Gurney law, the current density is given by is given by(Equation (2))

$$J = 9\varepsilon_0\varepsilon_r\mu V^2/8L^3 \quad (2)$$

where J is the current density, ε_0 is the permittivity of free-space, ε_r is the relative dielectric constant of the BHJ layer, μ is the hole mobility，L is the thickness of the BHJ layer, and V is the voltage drop across the device.[29] The J–V characteristics of the hole-only devices, fabricated with the structures of ITO/MoO3(8 nm)/PTB7-Th:$PC_{71}BM$(80 nm)/Au(80 nm), are shown in Fig. 9. The computed results show that the hole-mobility μ_h increases from 9.14×10^{-5} cm^2/Vs to 1.86×10^{-4} cm^2/Vs after methanol fluxing. The larger the μ_h, the better the pathways for carrier transportation. So the increased μ_h indicates that the charge transport properties are substantially improved after methanol fluxing. All these results show that the improved performance of OSCs after methanol fluxing is mainly due to the improved electronic performance.

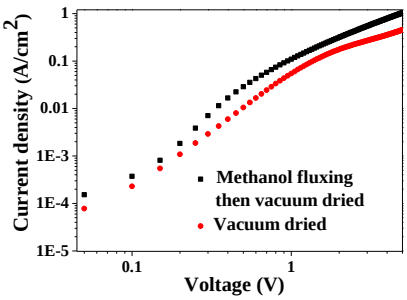

Fig. 9 J–V characteristics of PTB7-Th:$PC_{71}BM$ single carrier devices used for hole mobility measurement.

4. Conclusions

In summary, we have prepared the controllable gradient three-dimensional morphology by changing the volume fraction of DIO. After the formation of gradient three-dimensional structure, the whole performance of OSCs significantly improved, J_{SC} increases from 13.85 mA/cm^2 to 15.17 mA/cm^2 and FF increases from 62.86% to 65.68%, simultaneously, PCE increases from 6.79% to 7.67%. And the enhancement of device performance is attributed to the improved donor/acceptor interface, continuous pathways for carrier transportation, better domain size, enhanced IQE and higher hole-mobility with the formation of gradient three-dimensional structure.

Acknowledgments

The authors express the thanks to the New Century Excellent Talents in University, China (NCET-10-0220),the National Natural Science Foundation of China (51272022), the Specialized Research Fund for the Doctoral Program of Higher Education of China (20120009130005), and the Fundamental Research Funds for the Central Universities, China (2012JBZ001).

Notes and references

[a]Key Laboratory of Luminescence and Optical Information (Beijing Jiaotong University), Ministry of Education, Beijing, 100044, China
[b]Institute of Optoelectronics Technology, Beijing Jiaotong University, Beijing, 100044, China
[c] Corresponding author
Tel(Fax):86-10-51684462
E-mail address: slzhao@bjtu.edu.cn
Present address： Key Laboratory of Luminescence and Optical Information (Beijing Jiaotong University), Ministry of Education, Beijing, 100044, China
Electronic Supplementary Information (ESI) available. See DOI: 10.1039/b000000x/

1 C. P. Chen, Y. D. Chen and S. C. Chuang, Adv Mater, 2011, 23, 3859-3863.
2 L. Huo and J. Hou, Polymer Chemistry, 2011, 2, 2453.
3 D. H. Wang, J. S. Moon, J. Seifter, J. Jo, J. H. Park, O. O. Park and A. J. Heeger, Nano letters, 2011, 11, 3163-3168.
4 M. He, M. Wang, C. Lin and Z. Lin, Nanoscale, 2014, 6, 3984-3994.
5 J. Li, H. Yu and Y. Li, Nanoscale, 2011, 3, 4888.
6 G. Dennler, M. C. Scharber and C. J. Brabec, Advanced Materials, 2009, 21, 1323-1338.
7 B. V. Andersson, A. Herland and S. Masich, Nano letters, 2009, 9, 853-855.
8 L. M. Chen, Z. Hong, G. Li and Y. Yang, Advanced Materials, 2009, 21, 1434-1449.
9 A. J. Heeger, Adv Mater, 2014, 26, 10-27.
10 S. J. Lou, J. M. Szarko, T. Xu, L. Yu, T. J. Marks and L. X. Chen, Journal of the American Chemical Society, 2011, 133, 20661-20663.
11 H.-Y. Chen, J. Hou, S. Zhang, Y. Liang, G. Yang, Y. Yang, L. Yu, Y. Wu and G. Li, Nature Photonics, 2009, 3, 649-653.
12 S. Gunes, H. Neugebauer and N. S. Sariciftci, Chemical reviews, 2007, 107, 1324-1338.
13 H. Lu, B. Akgun and T. P. Russell, Advanced Energy Materials, 2011, 1, 870-878.
14 G. Li, Y. Yao, H. Yang, V. Shrotriya, G. Yang and Y. Yang, Advanced Functional Materials, 2007, 17, 1636-1644.
15 T.-Y. Chu, S. Alem, S.-W. Tsang, S.-C. Tse, S. Wakim, J. Lu, G. Dennler, D. Waller, R. Gaudiana and Y. Tao, Applied Physics Letters, 2011, 98, 253301.
16 Y. Liang, Z. Xu, J. Xia, S. T. Tsai, Y. Wu, G. Li, C. Ray and L. Yu, Adv Mater, 2010, 22, E135-138.
17 M. Campoy-Quiles, T. Ferenczi, T. Agostinelli, P. G. Etchegoin, Y. Kim, T. D. Anthopoulos, P. N. Stavrinou, D. D. Bradley and J. Nelson, Nature materials, 2008, 7, 158-164.
18 Z. Xiao, Y. Yuan, B. Yang, J. VanDerslice, J. Chen, O. Dyck, G. Duscher and J. Huang, Adv Mater, 2014, 26, 3068-3075.
19. J. Jo, S.-I. Na, S.-S. Kim, T.-W. Lee, Y. Chung, S.-J. Kang, D. Vak and D.-Y. Kim, Advanced Functional Materials, 2009, 19, 2398-2406.
20 A. Kumar, G. Li, Z. Hong and Y. Yang, Nanotechnology, 2009, 20, 165202.
21 A. J. Moulé and K. Meerholz, Advanced Functional Materials, 2009, 19, 3028-3036.
22 S. Berson, R. De Bettignies, S. Bailly and S. Guillerez, Advanced Functional Materials, 2007, 17, 1377-1384.
23 W. Ma, C. Yang, X. Gong, K. Lee and A. J. Heeger, Advanced Functional Materials, 2005, 15, 1617-1622.

24 W. Zeng, K. S. Yong, Z. M. Kam, F. Zhu and Y. Li, Applied Physics Letters, 2010, 97, 133304.
25 G. Dennler, K. Forberich, M. C. Scharber, C. J. Brabec, I. Tomiš, K. Hingerl and T. Fromherz, Journal of Applied Physics, 2007, 102, 054516.
26 P. Schilinsky, C. Waldauf and C. J. Brabec, Applied Physics Letters, 2002, 81, 3885.
27 H. Azimi, A. Senes, M. C. Scharber, K. Hingerl and C. J. Brabec, Advanced Energy Materials, 2011, 1, 1162-1168.
28 V. D. Mihailetchi, J. K. van Duren, P. W. Blom, J. C. Hummelen, R. A. Janssen, J. M. Kroon, M. T. Rispens, W. J. H. Verhees and M. M. Wienk, Advanced Functional Materials, 2003, 13, 43-46.
29 G. Malliaras, J. Salem, P. Brock and C. Scott, Physical Review B, 1998, 58, R13411.